

Longitudinal resolution in volumetric x-ray computerized tomography—Analytical comparison between conventional and helical computerized tomography

G. Wang and M. W. Vannier

Division of Radiology Research, Mallinckrodt Institute of Radiology, Washington University Medical School, Saint Louis, Missouri 63110

(Received 2 August 1993; accepted for publication 22 November 1993)

The primary advantage of helical computerized tomography (CT) is the capability of scanning a complete anatomical volume in a single breath hold. Due to the table motion and subsequent interpolation process, the slice sensitivity profile (SSP) in helical CT is worse than the response function of the detector array. In this paper, image longitudinal resolution in volumetric x-ray CT is analytically characterized, and a comparison made between conventional and helical CT. First, the SSPs are derived for both conventional and helical CT with the half-scan interpolation method under the condition that the table increment and detector collimation are the same. Then, the corresponding transfer functions are obtained for bandwidth determination, which directly describe the spatial resolution. Both one-tenth-cutoff and mean-square-root measures are used to quantify the bandwidth. Although it appears that broadening the SSP in helical CT could adversely affect longitudinal resolution, it is proved that for a given x-ray dose, helical CT allows substantially better longitudinal resolution than conventional CT due to its inherent retrospective reconstruction capability. To make full use of the potential of helical CT scan data, it is recommended that about five slices be reconstructed per table increment. Helical CT is superior in applications requiring a high longitudinal resolution.

Key words: volumetric imaging, helical CT, spiral CT, resolution, linear interpolation

I. INTRODUCTION

Helical computed tomography (helical CT, also referred to as spiral CT) is a major recent advance in x-ray CT for rapid volumetric scanning and has been clinically accepted. In helical CT, source rotation, patient translation, and data acquisition are continuously conducted. This imaging mode has the primary advantage of scanning a complete anatomical volume in a single breath hold, ensuring slice-to-slice contiguity.¹⁻⁴

Helical CT requires that planar projection sets be produced from raw helical scan data via interpolation. Among various interpolation techniques, linear interpolation is usually preferred due to its accuracy and efficiency. Typical linear interpolation techniques include full scan (FS), under scan (US), full-scan interpolation (FI or 360LI), half-scan (HS), half-scan interpolation (HI or 180LI) and half-scan extrapolation (HE) methods.³ The HI method is routinely used as the best linear interpolation method for most applications. In the HI method, a set of planar projection data is obtained via linearly interpolating neighboring raw data at the opposite orientations.

It has been demonstrated that the image quality of helical CT with the HI method is basically equivalent to that of conventional CT, except for some differences in the image noise, artifact patterns, and slice sensitivity profiles (SSPs).⁵⁻⁹ The image noise and artifacts have been studied and are beyond the scope of this paper. The SSP in helical CT is known to be a broadened version of the response function of the detector array,⁵⁻⁷ but the helical CT image longitudinal resolution has not been well investigated. Be-

cause the longitudinal resolution is an important issue in high-resolution volumetric x-ray CT imaging,¹⁰⁻¹⁷ we will perform an analysis in this paper.

In Sec. II, the SSPs in conventional and helical CT with the HI method are analytically derived under the condition that the table increment is equal to the detector collimation. Previously, the only analytically obtained SSP in helical CT (Ref. 5) is that associated with the FI method, which is inferior to the HI method and out-of-date. In Sec. III, the transfer functions (TFs) of the SSPs are found and the longitudinal bandwidths determined according to the one-tenth-cutoff and mean-square-root criteria, respectively. In Sec. IV, the practical implications of our findings are detailed. Section V concludes the paper.

II. SLICE SENSITIVITY PROFILES

A system point spread function (PSF) is determined by the detector array response function in conventional CT and by both the detector array response and table motion functions in helical CT. The slice sensitivity profile in CT is defined as the system PSF restricted to the line along the table motion direction and through the center of the gantry aperture. Therefore, the SSP reasonably describes the longitudinal resolution.

Let us assume that detectors in the array are densely arranged transversely and their response can be modeled as $f(z) = (1/D)\text{rect}(z/D)$, where z is the longitudinal coordinate, D is the longitudinal dimension of the detector collimation, and $\text{rect}(\cdot)$ is the rectangular function

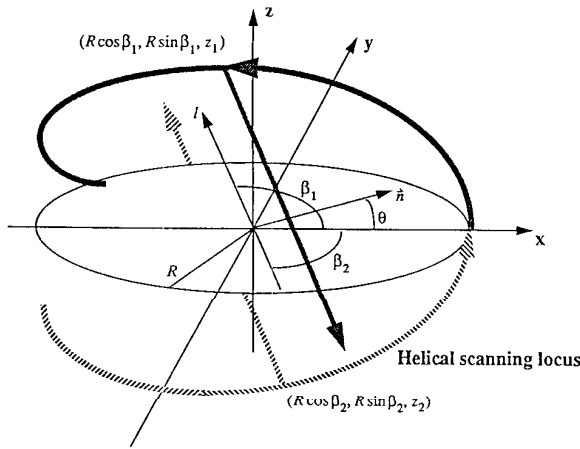


FIG. 1. Diagram showing variables and geometric relationships in the HI method.

$$\text{rect}(x) = \begin{cases} 1, & x \in [-\frac{1}{2}, \frac{1}{2}); \\ 0, & \text{otherwise.} \end{cases} \quad (1)$$

If the table increment is sufficiently small, it can be immediately obtained that the SSP in conventional CT, $p_c(z)$, is the same as the detector array response function

$$p_c(z) = \frac{1}{D} \text{rect}\left(\frac{z}{D}\right) \quad (2)$$

(projection and reconstruction are inverse operations to each other); otherwise, the SSP with a reconstruction interval kD in conventional CT, $p_{c,k}(z)$, is the convolution of the detector array response function $(1/D)\text{rect}(z/D)$ and the low-pass filtering function $(1/kD)\text{sinc}(\pi z/kD)$,

$$p_{c,k}(z) = \frac{1}{kD^2} \text{sinc}\left(\frac{\pi z}{kD}\right) * \text{rect}\left(\frac{z}{D}\right), \quad (3)$$

where k is the ratio of the table increment to the detector collimation, and

$$\text{sinc}(x) = \frac{\sin x}{x}. \quad (4)$$

Due to the table motion and resulting interpolation process, the SSP in helical CT is degraded compared to $p_c(z)$. Recognizing its performance and popularity, we will focus on the HI method in this study. Let θ denote the normal direction of a central projection ray l , β_1 , and β_2 the angles of its opposite rays make with respect to the axis x , z_1 , and z_2 the longitudinal coordinates of the x-ray source positions where the opposite rays radiate, and D the table increment, as illustrated in Fig. 1. Note that the table increment in helical CT has been assumed to be the same as the detector collimation, since in practice the pitch (the ratio of the increment to the collimation) is typically equal to one. Then, we have

$$\begin{cases} \beta_1 = \theta + \frac{\pi}{2}, \\ \beta_2 = \theta - \frac{\pi}{2}, \end{cases} \quad \theta \in \left[\frac{\pi}{2}, \frac{3\pi}{2}\right), \quad (5)$$

and

$$\begin{cases} z_1 = \frac{D}{2\pi} \beta_1 = \frac{D}{2\pi} \left(\theta + \frac{\pi}{2}\right), \\ z_2 = \frac{D}{2\pi} \beta_2 = \frac{D}{2\pi} \left(\theta - \frac{\pi}{2}\right). \end{cases} \quad (6)$$

Assume that an ideal impulse is located at the origin of the reconstruction coordinate system, the contribution to the reconstruction at a point $(0,0,-z)$, $p_h(-z,\theta)$, made from the projection values associated with the opposite rays is computed below in the HI method:

$$p_h(-z,\theta) = k_1 p_c(z+z_1) + k_2 p_c(z+z_2), \quad (7)$$

where

$$\begin{cases} k_1 = \frac{1}{\pi} \left(\frac{\pi}{2} - \theta\right), \\ k_2 = \frac{1}{\pi} \left(\frac{\pi}{2} + \theta\right). \end{cases} \quad (8)$$

Hence,

$$p_h(-z,\theta) = \frac{1}{\pi} \left(\frac{\pi}{2} - \theta\right) p_c\left[z + \frac{D}{2\pi} \left(\theta + \frac{\pi}{2}\right)\right] + \frac{1}{\pi} \left(\frac{\pi}{2} + \theta\right) p_c\left[z + \frac{D}{2\pi} \left(\theta - \frac{\pi}{2}\right)\right]. \quad (9)$$

Averaging $p_h(-z,\theta)$ with respect to θ , we have

$$p_h(-z) = p_h(z) = \frac{1}{\pi} \int_{-\pi/2}^{\pi/2} \frac{1}{\pi} \left(\frac{\pi}{2} - \theta\right) p_c\left[z + \frac{D}{2\pi} \left(\theta + \frac{\pi}{2}\right)\right] d\theta + \frac{1}{\pi} \int_{-\pi/2}^{\pi/2} \frac{1}{\pi} \left(\frac{\pi}{2} + \theta\right) p_c\left[z + \frac{D}{2\pi} \left(\theta - \frac{\pi}{2}\right)\right] d\theta. \quad (10)$$

Substituting $x = D\theta/2\pi$ into the above equation, it becomes

$$p_h(z) = \frac{1}{\pi^2} \int_{-D/4}^{D/4} \left(\frac{\pi}{2} - \frac{2\pi x}{D}\right) f\left(z+x+\frac{D}{4}\right) \frac{2\pi}{D} dx + \frac{1}{\pi^2} \int_{-D/4}^{D/4} \left(\frac{\pi}{2} + \frac{2\pi x}{D}\right) f\left(z+x-\frac{D}{4}\right) \frac{2\pi}{D} dx = \frac{2}{D} \int_{-D/4}^{D/4} \left(\frac{1}{2} - \frac{2x}{D}\right) f\left(z+x+\frac{D}{4}\right) dx + \frac{2}{D} \int_{-D/4}^{D/4} \left(\frac{1}{2} + \frac{2x}{D}\right) f\left(z+x-\frac{D}{4}\right) dx. \quad (11)$$

Introducing $g_1(x)$ and $g_2(x)$ as follows:

TABLE I. One-tenth-cutoff bandwidth in conventional CT as a function of the table increment kD , where D is the detector collimation and was set to 1, $\tilde{u}_c \equiv \tilde{u}_{c,e}$.

| | | | | | | | | | | | |
|-------------------|------------|-------|-------|-------|-------|-----|-------|-------|-------|-------|------|
| k | ϵ | 0.2 | 0.4 | 0.6 | 0.8 | 1.0 | 1.2 | 1.4 | 1.6 | 1.8 | 2.0 |
| $\tilde{u}_{c,k}$ | 0.908 | 0.908 | 0.908 | 0.833 | 0.625 | 0.5 | 0.417 | 0.357 | 0.312 | 0.278 | 0.25 |

$$g_1(x) = \begin{cases} \frac{1}{D} - \frac{4x}{D^2}, & x \in \left[-\frac{D}{4}, \frac{D}{4}\right]; \\ 0, & \text{otherwise,} \end{cases} \quad (12)$$

and

$$g_2(x) = \begin{cases} \frac{1}{D} + \frac{4x}{D^2}, & x \in \left[-\frac{D}{4}, \frac{D}{4}\right]; \\ 0, & \text{otherwise,} \end{cases} \quad (13)$$

it is obtained that

$$\begin{aligned} p_h(z) &= \int_{-\infty}^{\infty} g_1(x) f\left(z+x+\frac{D}{4}\right) dx \\ &\quad + \int_{-\infty}^{\infty} g_2(x) f\left(z+x-\frac{D}{4}\right) dx \\ &= \int_{-\infty}^{\infty} g_1\left(x-z-\frac{D}{4}\right) f(x) dx \\ &\quad + \int_{-\infty}^{\infty} g_2\left(x-z+\frac{D}{4}\right) f(x) dx \\ &= \int_{-\infty}^{\infty} \left[g_1\left(x-z-\frac{D}{4}\right) + g_2\left(x-z+\frac{D}{4}\right) \right] f(x) dx. \end{aligned} \quad (14)$$

Equating $g(z-x)$ to $g_1(x-z-D/4) + g_2(x-z+D/4)$, it follows that

$$g(x) = \begin{cases} \frac{2}{D} + \frac{4x}{D^2}, & x \in \left[-\frac{D}{2}, 0\right); \\ \frac{2}{D} - \frac{4x}{D^2}, & x \in \left[0, \frac{D}{2}\right]; \\ 0, & \text{otherwise.} \end{cases} \quad (15)$$

Therefore,

$$p_h(z) = g(z) * f(z). \quad (16)$$

Here, $g(*)$ is referred to as the table motion function in the HI method. In other words, the SSP in helical CT, $p_h(z)$, is the convolution of the detector array response and table motion functions. Similarly, the SSP with a reconstruction interval kD in helical CT, $p_{h,k}(z)$, is the convolution of $p_h(z)$ and $1/kD \text{sinc}(\pi z/kD)$, that is

$$p_{h,k}(z) = \frac{1}{kD} \text{sinc}\left(\frac{\pi z}{kD}\right) * g(z) * f(z). \quad (17)$$

III. LONGITUDINAL BANDWIDTHS

While the SSP completely describes the longitudinal image resolution, the transfer function (the Fourier transform of the SSP) possesses the same information content;

both approaches are equivalent. In this study, it is more convenient to work in the Fourier domain, because the reconstruction interval in CT can be considered as a sampling step, whose effect is of an ideal low-pass filter. In the Fourier domain, the spatial resolution is typically parametrized as the bandwidth (a signal can be fully recovered if its bandwidth stays within the bandwidth of the imaging process). Among various definitions of bandwidth, both the one-tenth-cutoff and mean-square-root measures are used.

A. Transfer functions

A Fourier transform pair¹⁸ is denoted as

$$f(x) \Leftrightarrow F(u) \quad (18)$$

with the definitions

$$F(u) = \int_{-\infty}^{\infty} f(x) e^{-i2\pi ux} dx, \quad (19)$$

and

$$f(x) = \int_{-\infty}^{\infty} F(u) e^{i2\pi ux} du. \quad (20)$$

Using the known Fourier transform relationships¹⁹

$$\text{rect}(x) \Leftrightarrow \text{sinc}(\pi u), \quad (21)$$

$$\text{tri}(x) \Leftrightarrow \text{sinc}^2(\pi u), \quad (22)$$

where

$$\text{tri}(x) = \begin{cases} 1+x, & x \in [-1, 0); \\ 1-x, & x \in [0, 1]; \\ 0, & \text{otherwise,} \end{cases} \quad (23)$$

and the properties that

$$f(x/a) \Leftrightarrow aF(au), \quad \text{where } a \text{ is a scaling factor,} \quad (24)$$

$$F(x) \Leftrightarrow f(u), \quad \text{if } f(x) \text{ is an even function,} \quad (25)$$

the transfer functions $P_c(u)$, $P_{c,k}(u)$, $P_h(u)$, and $P_{h,k}(u)$, corresponding to $p_c(z)$, $p_{c,k}(z)$, $p_h(z)$, and $p_{h,k}(z)$, respectively, can be shown to be the following:

$$P_c(z) = \text{sinc}(\pi Du), \quad (26)$$

$$P_{c,k}(u) = \text{sinc}(\pi Du) \text{rect}(kDu), \quad (27)$$

$$P_h(u) = \text{sinc}^2(\pi Du/2) \text{sinc}(\pi Du), \quad (28)$$

$$P_{h,k}(u) = \text{sinc}^2(\pi Du/2) \text{sinc}(\pi Du) \text{rect}(kDu). \quad (29)$$

TABLE II. One-tenth-cutoff bandwidth in helical CT as a function of the reconstruction interval kD , where D is the detector collimation and was set to 1, $\tilde{u}_h \equiv \tilde{u}_{h,\epsilon}$.

| | | | | | | | | | | | |
|-------------------|------------|-------|-------|-------|-------|-----|-------|-------|-------|-------|------|
| k | ϵ | 0.2 | 0.4 | 0.6 | 0.8 | 1.0 | 1.2 | 1.4 | 1.6 | 1.8 | 2.0 |
| $\tilde{u}_{h,k}$ | 0.838 | 0.838 | 0.838 | 0.833 | 0.625 | 0.5 | 0.417 | 0.357 | 0.312 | 0.278 | 0.25 |

B. One-tenth-cutoff bandwidths

Given a TF, its one-tenth-cutoff bandwidth can be found out by setting it to 0.1 and solving the equation on the interval of the main lobe. Because in some cases we cannot obtain closed-form solutions to the involved non-linear equations, the software tool MATHEMATICA™ was utilized to find the numerical roots. Tables I and II list the bandwidths in conventional and helical CT as a function of k ; kD is the table increment in conventional CT and reconstruction interval in helical CT (D is the detector collimation and was set to one in the computation without loss of generality). Note that the one-tenth-cutoff bandwidths $\tilde{u}_c \equiv \tilde{u}_{c,\epsilon} = \lim_{\epsilon \rightarrow 0} \tilde{u}_{c,\epsilon}$ and $\tilde{u}_h \equiv \tilde{u}_{h,\epsilon} = \lim_{\epsilon \rightarrow 0} \tilde{u}_{h,\epsilon}$.

C. Mean-square-root bandwidths

The mean-square-root of a Fourier power spectrum is another reasonable measure of the bandwidth.^{20,21} The mean-square-root bandwidth \bar{u} of a TF $F(u)$ is defined as

$$\bar{u}^2 = \frac{\int_0^\infty u^2 |F(u)|^2 du}{\int_0^\infty |F(u)|^2 du} \tag{30}$$

In our computation, some integrals with singularities and infinite limits were involved. MATHEMATICA™ was used with proper care to express the integrals in terms of standard functions such as the sinc integral and then to determine the integral values. Tables III and IV list the bandwidths in conventional and helical CT as a function of k ; kD is again the table increment and reconstruction interval in conventional and helical CT ($D=1$ in the computation). Note that the mean-square-root-bandwidths $\bar{u}_c \equiv \bar{u}_{c,\epsilon} = \lim_{\epsilon \rightarrow 0} \bar{u}_{c,\epsilon}$ and $\bar{u}_h \equiv \bar{u}_{h,\epsilon} = \lim_{\epsilon \rightarrow 0} \bar{u}_{h,\epsilon}$.

IV. PRACTICAL IMPLICATIONS

The longitudinal resolution depends on both the detector collimation and table increment. Suppose the table increment is sufficiently small (a small fraction of the collimation), the longitudinal resolution is solely determined by the detector array response function in conventional CT and then reaches its theoretically possible maximum. With the table increment being equal to the collimation in helical CT, even the reconstruction interval is sufficiently small, the longitudinal resolution in helical CT would not be as good as the maximum possible one in conventional CT. Similarly, if the table increment in both conventional and

helical CT are the same and equal to the reconstruction interval in helical CT, the longitudinal resolution in helical CT would not be favorably comparable to that in conventional CT.

These facts could lead to the erroneous impression that the longitudinal resolution in conventional CT is superior. However, the above arguments overlook two important factors. First, a sufficiently small table increment results in a very large x-ray dose, which is practically impossible in general. As a result, the maximum possible longitudinal resolution in conventional CT (u_c) is seldom reached, and the real longitudinal resolution is then the low-pass filtered version ($u_{c,k}$) of the maximum possible one (u_c). Second, the reconstruction interval in helical CT can be made sufficiently fine only at cost of computing resources. Setting the reconstruction interval to the table increment is just one of possible choices. To compare longitudinal resolution in conventional and helical CT, it is only fair to require not only the collimation but also the x-ray dose be the same. The identical x-ray dose means equal table increments. In conventional CT, the reconstruction interval is the same as the table increment, and the retrospective reconstruction is achieved via Shannon’s interpolation. In helical CT, the reconstruction interval is arbitrary, and it is feasible to reach the maximum possible longitudinal bandwidth u_h . Therefore, in evaluating the longitudinal resolution, it is $u_{c,1}$ (the longitudinal bandwidth in conventional CT with the same table increment as the detector collimation) and u_h (the maximum possible longitudinal bandwidth in helical CT) that should be compared.

Based on the bandwidth computations, the longitudinal resolution in helical CT is superior to that in conventional CT, as the helical CT bandwidths are substantially larger than the conventional CT counterparts [$\tilde{u}_h(0.838) > \tilde{u}_{c,1}(0.5)$ and $\bar{u}_h(0.297) > \bar{u}_{c,1}(0.256)$]. To utilize helical CT to its full capability, it is recommended that about five slices be reconstructed per table increment [$\tilde{u}_{h,0.2}(0.838) = \tilde{u}_h(0.838)$ and $\bar{u}_{h,0.2}(0.296) \approx \bar{u}_h(0.297)$]. To achieve the same longitudinal resolution in conventional CT, about a 30% slice overlap is needed (a 60% more x-ray dose) [$\tilde{u}_{c,0.6}(0.833) \approx \tilde{u}_h(0.838)$ and $\bar{u}_{c,0.8}(0.296) \approx \bar{u}_h(0.297)$].

V. CONCLUSION

We have formulated the SSPs and TFs for both conventional and helical CT with the half-scan interpolation

TABLE III. Mean-square-root bandwidth in conventional CT as a function of the table increment kD , where D is the detector collimation and was set to 1, $\bar{u}_c = \bar{u}_{c,\epsilon}$.

| | | | | | | | | | | | |
|-----------------|------------|-------|-------|-------|-------|-------|-------|-------|-------|-------|------|
| k | ϵ | 0.2 | 0.4 | 0.6 | 0.8 | 1.0 | 1.2 | 1.4 | 1.6 | 1.8 | 2.0 |
| $\bar{u}_{c,k}$ | ∞ | 0.514 | 0.349 | 0.331 | 0.296 | 0.256 | 0.222 | 0.194 | 0.173 | 0.155 | 0.14 |

TABLE IV. Mean-square-root bandwidth in helical CT as a function of the reconstruction interval kD , where D is the detector collimation and was set to 1, $\bar{u}_{h,k} \equiv \bar{u}_{h,\epsilon}$.

| k | ϵ | 0.2 | 0.4 | 0.6 | 0.8 | 1.0 | 1.2 | 1.4 | 1.6 | 1.8 | 2.0 |
|-----------------|------------|-------|-------|-------|-------|-------|-------|-------|-------|-------|-------|
| $\bar{u}_{h,k}$ | 0.297 | 0.296 | 0.294 | 0.291 | 0.272 | 0.242 | 0.213 | 0.189 | 0.169 | 0.152 | 0.138 |

method, and computed the corresponding bandwidths according to the one-tenth-cutoff and mean-square-root criteria. In addition to the advantage of short data acquisition time, we have analytically recognized another major advantage of helical CT—better longitudinal image resolution, compared to conventional CT. To make full use of helical CT scan data, about five slices should be reconstructed per table increment. We recommend helical CT in applications requiring high longitudinal resolution, such as skull base and temporal bone imaging, and lesion detection and measurement.

ACKNOWLEDGMENTS

The authors would like to thank Dr. W. Kalender and Dr. A. Polacin at Siemens UB Med. (Erlangen, Germany) for the discussion on spiral/helical CT, Dr. G. Fletcher at Mallinckrodt Institute of Radiology for the advice on using MATHEMATICA™, and reviewers for thoughtful comments. This work was supported in part by Siemens Medical Systems, Inc.

¹Y. Bresler and C. J. Skrabacz, "Optimal interpolation in helical scan computed tomography," *Proc. ICASSP* **3**, 1472–1475 (1989).

²W. A. Kalender, W. Seissler, E. Klotz, and P. Vock, "Spiral volumetric CT with single-breath-hold technique, continuous transport, and continuous scanner rotation," *Radiology* **176**, 181–183 (1990).

³C. R. Crawford and K. F. King, "Computed tomography scanning with simultaneous patient translation," *Med. Phys.* **17**, 967–982 (1990).

⁴H. Rigaults, G. Marchal, A. L. Baert, and R. Hupke, "Initial experience with volume CT scanning," *J. Comput. Assist. Tomog.* **14**, 675–682 (1990).

⁵W. A. Kalender and A. Polacin, "Physical performance characteristics of spiral CT scanning," *Med. Phys.* **18**, 910–915 (1991).

⁶A. Polacin, W. A. Kalender, and G. Marchal, "Evaluation of section sensitivity profiles and image noise in spiral CT," *Radiology* **185**, 29–35 (1992).

⁷J. A. Brink, J. P. Heiken, D. M. Balfe, S. S. Sagel, J. DiCroce, and M. W. Vannier, "Spiral CT: Decreased spatial resolution *in vivo* due to broadening of section-sensitivity profile," *Radiology* **185**, 469–474 (1992).

⁸G. Wang and M. W. Vannier, "Helical CT image noise—Analytical results," *Med. Phys.* **20**, 1635–1640 (1993).

⁹G. Wang and M. W. Vannier, "Stair-step artifacts in three-dimensional helical CT: An experimental study," *Radiology* (in press).

¹⁰D. Ney, E. Fishman, A. Kawashima, D. Robertson, and W. Scott, "Comparison of helical and serial CT with regard to three-dimensional imaging of musculoskeletal anatomy," *Radiology* **185**, 865–869 (1992).

¹¹G. H. Esselman, J. M. Coticchia, F. J. Wippold, II, J. M. Frederickson, M. W. Vannier, and J. G. Neeley, "Test fitting an implantable hearing aid using three dimensional CT scans of the temporal bone," *Am. J. Otolaryngology* (submitted) (also presented at the Annual Meeting of the American Otological Society, Los Angeles, CA, 1993).

¹²M. W. Skinner, D. R. Ketten, M. W. Vannier, G. A. Gates, R. L. Yoffie, and W. A. Kalender, "A technique for determining the position of Nucleus™ implant electrodes in the inner ear," *Am. J. Otolaryngology* (in press).

¹³M. W. Vannier and G. Wang, "Spiral CT refines temporal bone imaging," *Diagn. Imaging* **15**, 116–121 (1993).

¹⁴P. Costello, W. Anderson, and D. Blume, "Pulmonary nodule: Evaluation with spiral volumetric CT," *Radiology* **179**, 875–876 (1991).

¹⁵S. Heywang-Koekrunner, B. Lommatzsch, U. Fink, and B. Mayr, "Comparison of spiral and conventional CT in the detection of pulmonary nodules," *Radiology* **185**(P), 131 (1992).

¹⁶D. Dupuy, P. Costello, and C. Ecker, "Spiral CT of the pancreas," *Radiology* **183**, 815–818 (1992).

¹⁷M. Remy-Jardin, J. Remy, F. Giraud, and C. Marquette, "Pulmonary Nodules: Detection with thick-section spiral CT versus conventional CT," *Radiology* **187**, 513–520 (1993).

¹⁸A. C. Kak and M. Slaney, *Principles of Computerized Tomographic Imaging* (IEEE, New York, 1987).

¹⁹A. K. Jain, *Fundamentals of Digital Image Processing* (Prentice-Hall, Englewood Cliffs, NJ, 1989), Chap. 2.

²⁰D. Gabor, "Theory of communication," *J. IEE* **93**, 429–457 (1946).

²¹O. Rioul and M. Vetterli, "Wavelets and signal processing," *IEEE Signal Process.* **8**, 14–38 (1991).